

NONLINEAR STATIC AEROELASTIC BEHAVIOR OF COMPOSITE MISSILE FIN WITH INTERLAMINAR DAMAGE

Özge Özkaya¹ and Altan Kayran²
Middle East Technical University
ANKARA, Turkey

ABSTRACT

Nonlinear static aeroelastic behavior of a basic composite missile fin is analyzed by means of two-way coupled FSI simulation and the effects of composite damages are presented. The configuration has been simulated by coupling the two commercial solvers ANSYS CFX for the fluid mechanical simulation with ANSYS Mechanical for the structural simulation. 3D composite fin geometry is constructed using ANSYS ACP tool. Interlaminar damage cases were investigated and the influence of the damage locations on the static aeroelastic behavior is discussed. It is shown that for the cases investigated, leading and trailing edge delamination in the compressive zone of the composite laminate of the fin are more critical in terms of their effect on the static aeroelastic response of the composite missile fin under the flow conditions analyzed.

INTRODUCTION

Today, in the missile systems the trend is toward greater use of composites, like in the aircraft industry, due to composites' superior strength to weight ratio. For a missile, lighter weight means extended range capability. For a missile that is launched from aircraft, lighter weight improves the carrying capacity of the aircraft. In addition, since lighter weight of the payload improves the fuel capacity of the aircraft, the range of the aircraft will also increase. Therefore, most of the components of missile can be produced in composites including the seeker, warhead, guidance electronics and so on. As a particular case, composite fin is investigated in this study.

As well as the weight advantage that the composites offer, there are also disadvantages of the composites. It is known that, composite structures are prone to failure either because of the defects which may occur inside the structure during the manufacturing or operation. Damages may alter the static aeroelastic behavior of the missile fin and in turn the missile to which the fin is attached to. Changes in the static aeroelastic behavior of the missile may cause performance losses especially in missiles which do not have a guidance system. Even for guided missiles, the change of the static aeroelastic behavior due to damages in the composite structure may affect the missile performance adversely. Therefore in this study,

¹ M.S Student in Aerospace Engineering Department, METU, Email: e174723@metu.edu.tr

² Prof. Dr. in Aerospace Engineering Department, METU, Email: akayran@metu.edu.tr

the effect of damages in the composite missile fin structure on the static aeroelastic behavior of the fin is investigated.

For a composite lifting surface, detecting the damage; evaluating the initiation and evolution of the damage is of great importance. However, understanding the aeroelastic behavior once the wing is damaged is also very important. While many studies have been done for the first issue; less research is available for the aeroelastic studies. From the early studies, Bauchau and Loewy [Bauchau and Loewy, 1997] studied the nonlinear aeroelastic effects in damaged composite aerospace structures. The results show that, the presence of matrix micro-crack damages and localized delamination do not have a significant influence on the flutter speed, however, this damage can induce a limit cycle behavior at airspeeds below the flutter speed. Kim et al. [Kim, Atluri and Loewy, 1998] investigated the flutter response and aeroelastic stability of a composite plate with microcracks in the matrix. The reduced elastic moduli due to the microcracking in the matrix of the composites are given as a function of crack density distribution. The numerical results indicate the loss in aeroelastic stability due to the nonlinear bimodular oscillation and the reduction of the bending stiffness.

The efforts of Strganac and Kim [Strganac and Kim, 1996] have addressed the dynamic response and stability of damage composite plates under aeroelastic loads. The crack density parameter is defined for the microcracks damages in the matrix. The results are shown to be highly dependent upon the distribution and accumulation of damage.

Eastepp [Eastepp, Venkayya and Tishler, 1984] investigated the degradation of the divergence speed of the forward swept wings with damaged composite skin. The various damage cases considered along with the decrease of divergence speed.

Wang and Inman [Wang and Inman, 2007] studied the crack induced changes in the aeroelastic boundaries of an unswept composite wing. Changes in flutter and divergence speeds are compared with respect to the crack ratio and location.

The aeroelastic characteristics of a cantilevered composite panel with an edge crack are investigated by Wang et al [Wang, Inman and Farrar, 2005]. They investigated the variation of the divergence and flutter speed with respect to the crack ratio, its location and the fiber angle. Results show that depending on the fiber orientation, the crack may or may not reduce the divergence and flutter speed.

In present work, the main objective is to investigate the aeroelastic response due to the presence of delamination in the composite fin. The effect of the location of the delamination on the deformation of the fin and aerodynamic coefficients are examined in one way and coupled two way aeroelastic analyses.

METHOD

Fluid Structure Interaction (FSI)

The study of the behavior of structures in contact with the fluid is the field of Fluid Structure Interaction (FSI). The interaction between fluids and solids can only be calculated using laws and equations from different physical disciplines. Therefore, two separate solvers, one for the fluid (CFD) and one for the structure (FEM) are needed for the solution of such FSI simulations. When the results of the CFD analysis are transferred and applied as loads to the mechanical model, this approach is called as one-way FSI analysis. In one way analysis, resulting displacements are not fed back to the CFD analysis. When the influence of deformed structure is captured, the approach is called as two-way FSI analysis. In the two-way approximation, the CFD results are transferred to the structural model as loads whereas the subsequently calculated displacements at the interface are transferred back to the CFD analysis. In this study, the coupling is provided by CFX [Ansys Inc., 2013] which is a commercial CFD software working with the ANSYS Mechanical solver. The static aeroelastic behavior of the AGARD Wing 445.6 is studied using two-way approach to validate the procedure by comparing with the results available in the literature.

AGARD Wing 445.6 Case:

AGARD Wing 445.6 that is used in wind tunnel experiments for its flutter characteristics in the Langley Transonic Dynamics Tunnel is a well-known test case for aeroelastic problems [Yates, 1995]. AGARD 445.6 test case is a low-aspect-ratio swept wing with a NACA 65A004 airfoil. The AGARD 445.6 Wing panel is modeled in Ansys-Workbench.

ANSYS has different solid elements available in its element library. A higher-order element that is SOLID186 [Ansys Inc., 2013] is used to model the wing. SOLID186 is a 3-D 20-node solid element that exhibits quadratic displacement behavior. The element is defined by 20 nodes having three degrees of freedom per node: translations in the nodal x, y, and z direction.

The finite element model of AGARD Wing 445.6 can be seen in Figure 1.

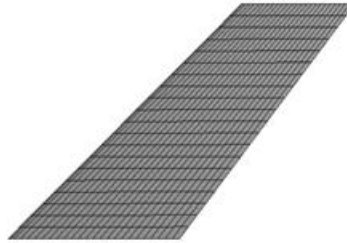


Figure 1: Finite Element Models of the AGARD Wing 445.6

The simulation is performed using the static structural (Ansys-Mechanical) and fluid flow (CFX-Pre) solvers of Ansys. Mesh, boundary conditions, analysis options and output options are defined independently for both models. Ansys Structure is the master process that controls the transient time step, interface mapping, interface convergence checks, load transfer, etc. However, all these settings are defined in CFX-Pre. The Ansys mapping is done to interpolate loads between nonconformal meshes on either side of the fluid-solid interface. In the Mechanical Application, the structural part is meshed while the fluid part is suppressed. Likewise, in the fluid model, fluid domain is meshed while the structural part is suppressed. Appropriate names are assigned to all inlet, outlet and side surfaces as well as the surface of the structure in the mesh generation part. Then the corresponding boundary conditions for the named surfaces are specified in CFX-Pre. The boundary type 'wall' is given for the surface of the structure with mass and momentum option of 'no-slip wall'. This condition indicates that the fluid moves along the wall. Inlet velocity and outlet pressure is defined in CFX. The isometric view of the domain used is given in Figure 2.

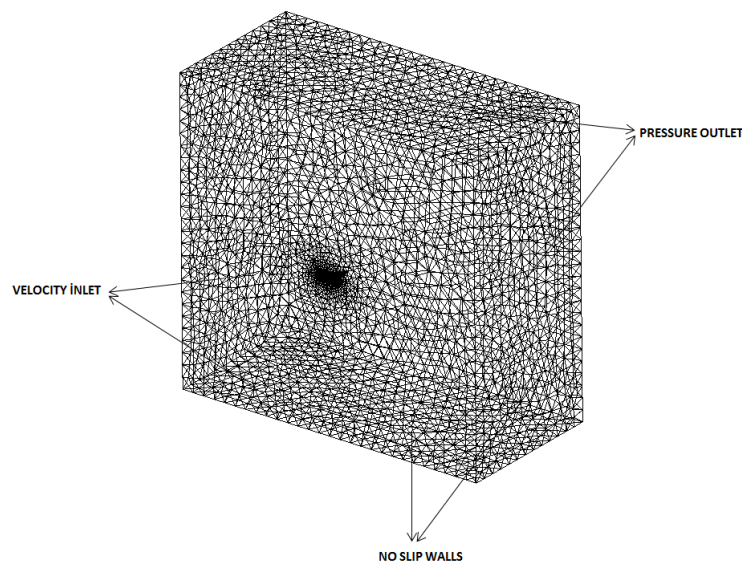


Figure 2: Fluid Domain and Boundaries

Nonlinear static aeroelasticity analysis is an iterative solving process. It is started by the aerodynamic calculation of the initial rigid wing model. The deformation under the

aerodynamic load is obtained after importing the loads to the structural mode and performing structure analysis. Then the mesh for the next aerodynamic calculation is regenerated based on the deformed wing configuration. Structural analysis is carried out again until both aerodynamic load and deformation converge within a prescribed tolerance or the maximum iteration number is reached.

For the Agard Wing, at the end of the static aeroelastic analysis, the reduction of the lift coefficient C_L for the $M=0.85$ and $\alpha=5^\circ$ flow condition is shown in Figure 3.

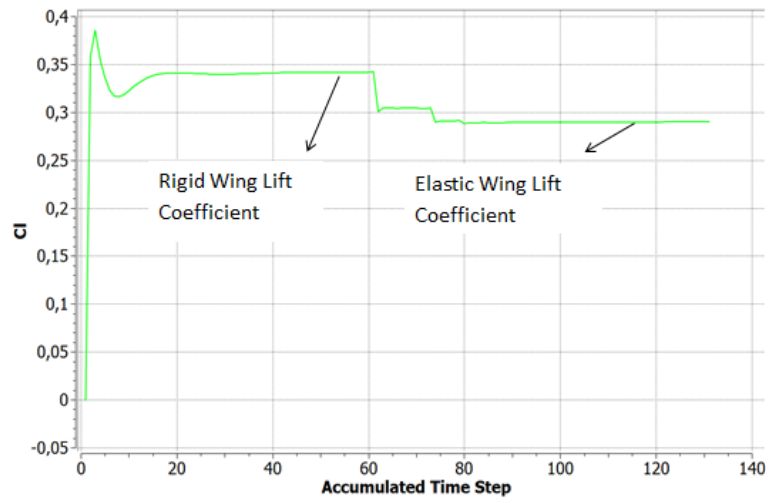


Figure 3: Lift Coefficients for Rigid and Elastic Wings

The results of the present analysis are compared with the study of Cai [Cai, Liu, Tsai and Wong, 2001] in Table 1. Table 1 shows that Cai's Navier Stokes solution results agreed well with the results of the present study.

Table 1: Comparison of Rigid and Elastic Wing Lift Coefficients

	Rigid Wing Lift Coefficient	Elastic Wing Lift Coefficient	% Reduction
Present Study	0.335	0.284	15.22
Cai (N.S)	0.339	0.288	15.04

The pressure coefficient distributions (C_p) of the rigid and elastic wing at the 67% and the 34% spanwise locations are given in Figure 4.

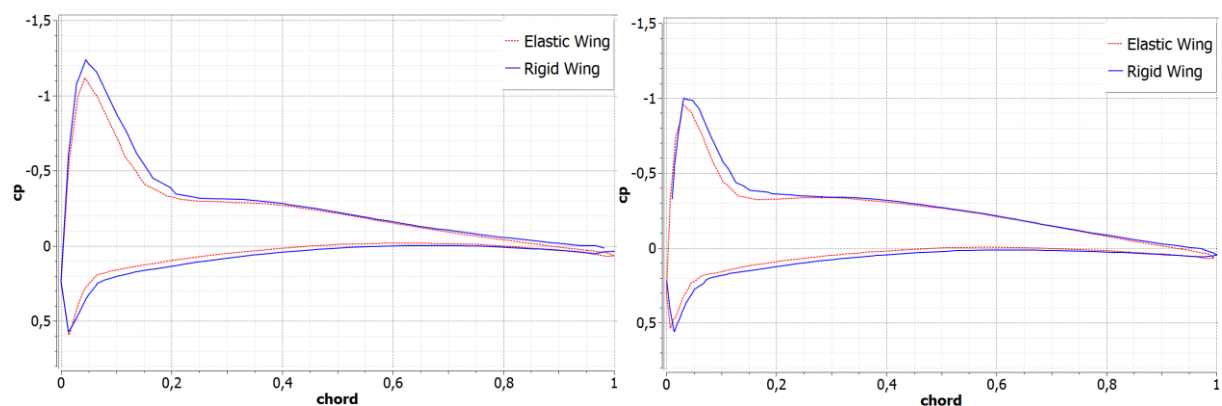


Figure 4: Rigid and Elastic Wing C_p Distributions at 67% Span (Left) and 34% Span (Right) Location

It can be seen in Figure 4 that, there is a reduction in the maximum C_p values for the elastic wing. The suction pressure at the upper surface of the elastic wing is reduced compared to the rigid wing. This reduction results in a decrease in the lift as shown in Figure 3.

The displacement results for the leading and the trailing edge at the end of the one way and two way analysis are shown in Figure 5.

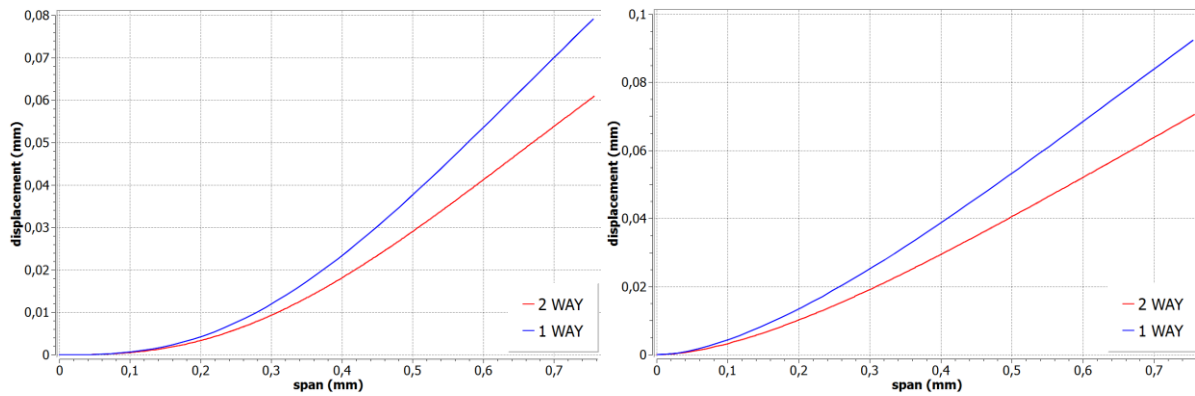


Figure 5 : Deflection of the Leading Edge (Right) and Trailing Edge (Left) of the AGARD Wing 445.6

In Figure 5, it can be seen that the deflection of the wing is reduced in the 2-way analysis. The backward shape of the AGARD wing leads to wash-out that reduces the angle of attack of the wing. The higher displacement of the trailing edge compared to leading edge can also be seen in Figure 5. The reduction of the angle of attack leads lift to decrease that result in a difference in displacements between one way and two way solutions. This aeroelastic effect can be seen with two way analysis.

Nonlinear Static Aeroelastic Analysis of the Composite Missile Fin

To model the missile structure that is used in this study, simple trapezoidal fin geometry is modeled by constructing the plies using the ANSYS ACP tool. The solid fin geometry consists of SOLID185 [Ansys Inc., 2013] 3-D Structural Solid element which is defined by eight nodes having three degrees of freedom at each node: translations in the nodal x, y, and z directions. Uni-Directional Epoxy Carbon is used as the ply material and the 0.5 mm thick plies are constructed using $[0^\circ/0^\circ/45^\circ/-45^\circ/90^\circ]_s$ stacking sequence as shown in Figure 6.

The orthotropic stress limits for this material are given in Table 2.

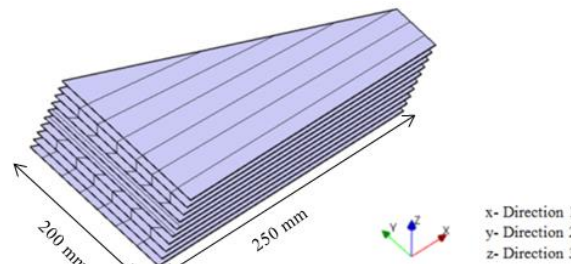


Figure 6: $[0^\circ/0^\circ/45^\circ/-45^\circ/90^\circ]_s$ Stacking Sequence of the Fin

Table 2: Stress Limits for Epoxy Carbon UD

Orthotropic Stress Limits (Mpa)		Orthotropic Elasticity (Mpa)	
Tensile x direction	2231	Young's Modulus xdirection	1.21e05
Tensile y direction	29	Young's Modulus ydirection	8600
Tensile z direction	29	Young's Modulus zdirection	8600
Compressive x direction	-1082	Poisson's Ratio xy	0.27
Compressive y direction	-100	Poisson's Ratio yz	0.4
Compressive z direction	-100	Poisson's Ratio xz	0.27
Shear xy	60	Shear modulus xy	4700
Shear yz	32	Shear modulus yz	3100
Shear xz	60	Shear modulus xz	4700

Same procedure as in the AGARD 445.6 wing analysis is followed for the two way analysis of the composite fin. The flow solution over the rigid fin is used as an initial condition of the aeroelastic iterations. Flow over the rigid fin is computed until the root mean square (RMS) residuals of the CFD variables fall below the prescribed tolerance value of 10^{-4} . Once the converged solution is obtained aeroelastic iterations start. The aerodynamic loads coming from CFD analysis are sent to the FEM solver to calculate the nodal displacements. Then, displacements are transferred to the flow domain (CFX) to obtain the aerodynamic loads on

the deformed structure. Iterations continue until the RMS value of the difference between the structural displacements of the two consecutive iterations is less than the prescribed tolerance of 10^{-4} m.

Nonlinear static aeroelastic analyses are done for the undamaged fin and fin with interlaminar damages and the results are compared in the following sections.

Undamaged Composite Fin:

At the end of the two-way aeroelastic solution, the change in the lift coefficient (C_L) for the $M=0.85$ and $\alpha=5^\circ$ flow condition is shown in Figure 7 for the rigid and elastic missile models.

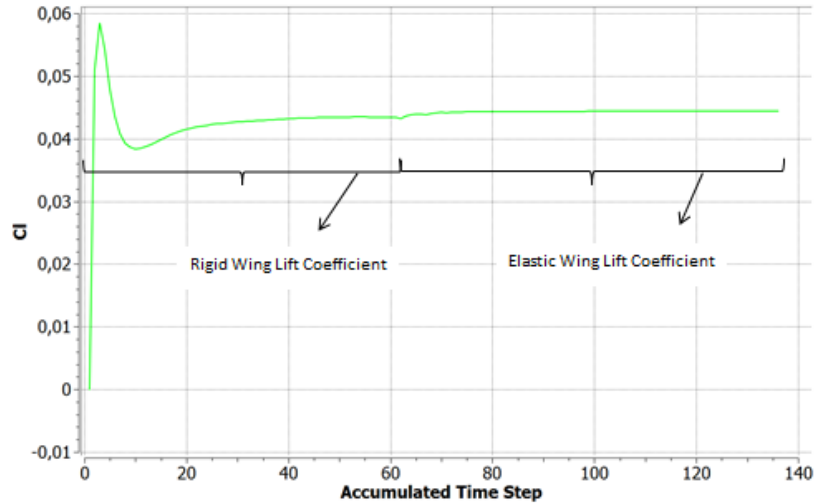


Figure 7: Convergence History of the Lift Coefficient (C_L) of the Rigid and the Elastic Undamaged Fin

It can be seen from Figure 7 that there is a little increase in the lift coefficient of the elastic composite fin compared to the rigid one. The lift coefficient result of the rigid fin is obtained as 0.0434 while elastic fin is obtained as 0.0444. In addition, sectional lift coefficient (C_l) distribution can be seen in Figure 8. It should be noted that since the composite fin studied is very rigid aeroelastic effect is minimal.

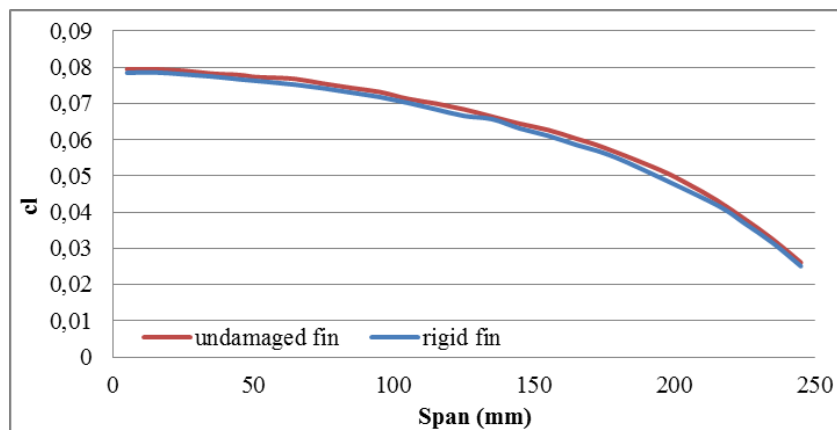


Figure 8: Spanwise Lift Coefficient (C_l) of the Rigid Fin vs. the Undamaged Fin

Converged deformation of the undamaged composite fin can be seen in Figure 9. Maximum tip deformation of the fin is 7.98 mm.

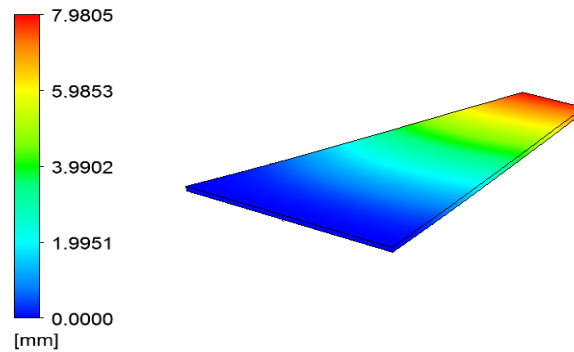


Figure 9: Deformation of the Undamaged Fin at the End of Two Way Analysis

In one way analysis, the maximum deformation of the fin is found as 7.6 mm. This little difference is because, in one way analysis the fluid pressure on the fin is transferred to the structural solver, but the displacement of the fin is not transferred back to the fluid solver. The fact that the deformation of the leading edge is higher than the deformation of the trailing edge leads to an increase in the angle of attack. In two way analysis, this increase in the angle of attack is taken into account by feeding back the deformation back to the fluid solver, resulting in increase in the lift and therefore increase in the displacement.

Pressure coefficient (C_p) distribution of the rigid and undamaged composite fin at the 50% and 96% span locations are shown in Figure 10.

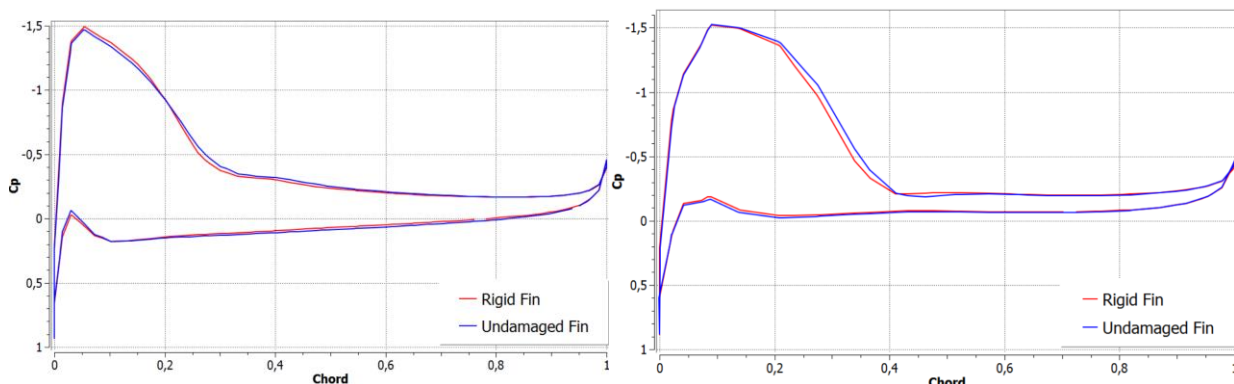


Figure 10: Pressure coefficient (C_p) distribution of the Undamaged Fin at the 50% (left) and 96% (right) span locations

It can be seen from the Figure 10 that, in spite of the little increase in the suction pressure for undamaged fin, C_p distributions for rigid and undamaged composite fin are very close to each other.

Composite Missile Fin with Interlaminar Damage

Interlaminar failure which occurs between adjacent layers is also called as delamination. Since the bonding of the adjacent layers only depends on matrix properties, cracks can form and propagate easily. Delamination can be analyzed by the cohesive zone method by inserting cohesive elements between the solid elements which model individual plies. According to the cohesive zone method, the stress transfer capacity between the two layers is not completely lost at the damage initiation; it is a progressive event governed by the progressive stiffness reduction. The behavior of the cohesive elements is characterized by the constitutive relation between the traction acting on the interface and the corresponding interfacial separation.

For the verification of the cohesive zone modeling, 3D model of a Double Cantilever Beam (DCB) specimen is constructed with the properties used in literature. Then, the delamination analysis results are compared with the analysis and test data of Travesa [Travesa, 2006].

The DCB specimen is 102 mm long while initial delamination is 32.9 mm. It is clamped at the end and a displacement of 4.5 mm is applied at the top and bottom edge. The boundary and load conditions of the DCB model are shown in Figure 11.

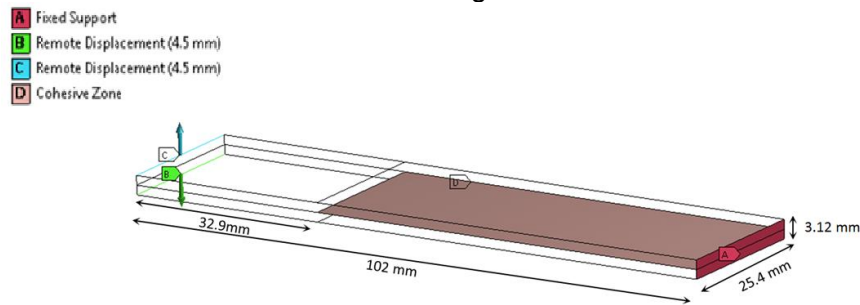


Figure 11: Dimensions, Boundary, Load Conditions and Cohesive Zone of DCB specimen

The finite element model of the DCB specimen is generated using ANSYS ACP tool. The material properties of the unidirectional AS4/PEEK carbon fiber reinforced composite which is used by Travesa [Travesa, 2006] is given in Table 3.

Table 3: Properties of Unidirectional As4/Peek Carbon Fiber Reinforced Composite [Travesa, 2006]

E_{11} (GPa)	$E_{22}=E_{33}$ (GPa)	$G_{12}=G_{13}$ (GPa)	G_{23} (GPa)	$\nu_{12}=\nu_{13}$	ν_{23}	G_{IC} (kJ/m ²)	G_{IIC} (kJ/m ²)
122.7	10.1	5.5	3.7	0.25	0.45	0.969	1.179

In this study, cohesive material behavior is implemented by using contact elements. For this purpose, TARGE170 (3D Target Segment Element) and CONTA174 (3D 8-Node Surface-to-Surface Contact) elements [Ansys Inc., 2013] that have zero thickness and can detect contact, separation, penetration and slip between a contact surface and a target surface is used. The bilinear cohesive zone material model is used for the analysis and the inputs are given as separation-distance based that is shown in Table 4.

Table 4: Properties of Cohesive Elements

Property	Value
Debonding Interface Mode	Mixed
Maximum Normal Contact Stress	80 MPa
Contact Gap at the Completion of Debonding	0.0242 mm
Maximum Equivalent Tangential Contact Stress	100 MPa
Tangential Slip at the Completion of Debonding	0.0236 mm
Artificial Damping Coefficient	0.01 s

Figure 12 shows the deformed shape of cantilever beam as a result of the application of 4.5 mm displacement in both directions at the tip of the DCB specimen.

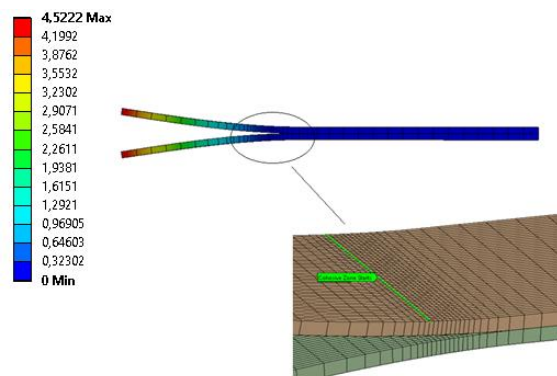


Figure 12: Total displacement of the DCB specimen, mm.

The comparison load-displacement curve of present analysis with the experimental and numerical results of Travesa's [Travesa, 2006] study is given in Figure 13.

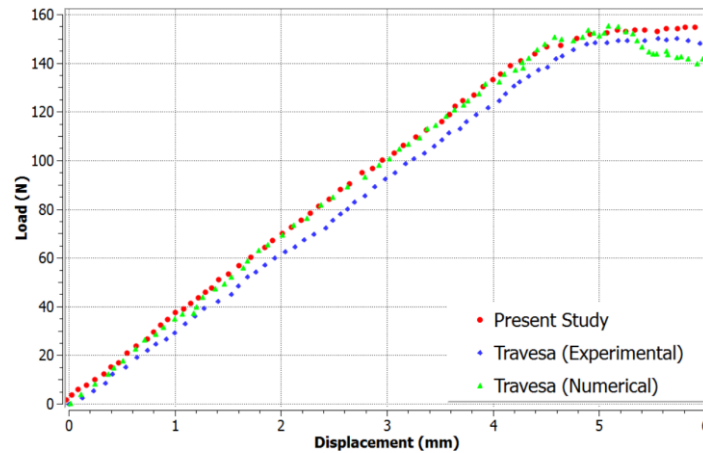


Figure 13: Load-Displacement curve of DCB specimen

From the load displacement curve it is seen that as the load reaches about 150 N, the gap between the layers reaches about 5 mm and damage starts to occur. From this point on, the cohesive material gradually loses its stiffness.

The results of the present study show good agreement with the experimental and numerical results of the study of Travesa [Travesa, 2006]. It should be noted that the cohesive elements in both studies are 8-node, zero thickness elements and used to connect 3 dimensional elements. However, in the present analysis, cohesive elements used are defined in the finite element code Ansys. In the study of Travesa [Travesa, 2006], the cohesive elements are implemented using a user-written subroutine in the finite element code in commercial software Abaqus.

In this study, interlaminar damages are created in the composite fin by placing cohesive interface layers at the upper ply interface of the fin since it gives the most critical results. Certain parts such as the leading edge, trailing edge, and the tip of the missile fin are left open which are typical locations where disbonds are very probable.

- Delamination in Upper Ply Interface of the Tip of the Fin:

In this case, delamination is modeled by leaving a width of 25 mm from the tip of the upper ply open while the remaining portion is bonded with cohesive elements and cohesive material properties given in Table 4 are used for the cohesive elements. Cohesive zone is placed between the upper ply and the second ply as shown in Figure 14.

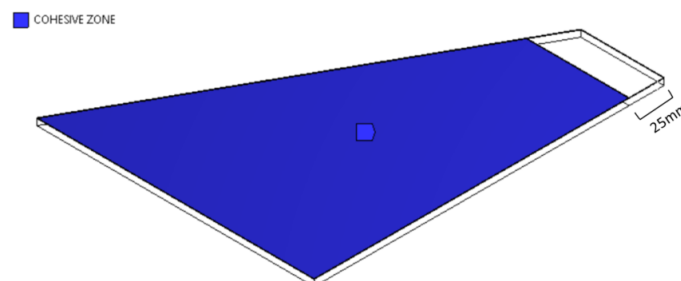


Figure 14: Upper Ply Delamination Model at the Tip of the Fin

For the fin with interlaminar damage at the tip of the fin, at the end of the two-way solution, the reduction of C_L for the $M=0.85$ and $\alpha=5^\circ$ flow condition is shown in Figure 16 for the rigid and elastic missile fin models.

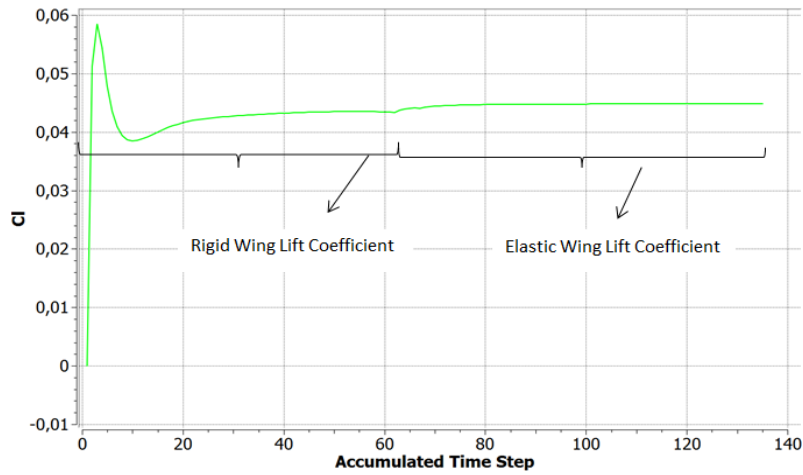


Figure 15: Convergence History of the Lift Coefficient of the Rigid and Elastic Fin with Tip Delamination

It can be seen from Figure 15 that, as in the case of undamaged fin, there is a little increase in the lift coefficient compared to the rigid one. The lift coefficient of the rigid fin is obtained as 0.0434 while for the composite fin with tip delamination; lift coefficient is obtained as 0.0448. The lift remains almost the same; there is only 3.2% increase. However, it is seen that, compared to the undamaged fin case, lift increases slightly.

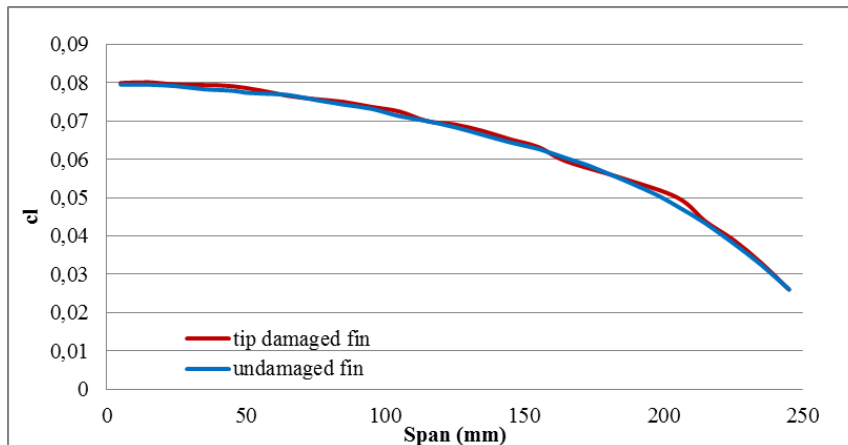


Figure 16: Spanwise Lift Coefficient (C_l) of the Undamaged Fin vs. the Fin with Tip Delamination

The spanwise lift coefficient of the rigid fin and the composite fin with tip delamination is shown in Figure 16. It is seen that sectional lift coefficients are almost the same as the undamaged fin.

The converged maximum deformation of the fin is 10 mm which is shown in Figure 17.

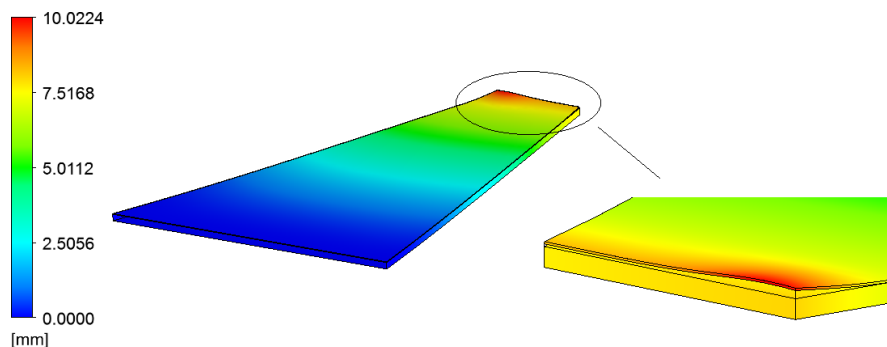


Figure 17: Aeroelastic Deformation of the Fin with Tip of the Upper Ply Delamination at the Tip of the Fin

At the end of one way analysis, the maximum deformation of the fin that has delamination in the upper ply interface of the tip is found as 9.32 mm. As a result of the two-way analysis, the maximum deformation increases about 7.3 %. As in the case of undamaged fin, the fact that the deformation of the leading edge is higher than the deformation of the trailing edge leads to an increase in the angle of attack. In two way analysis, this increase in the angle of attack is taken into account by feeding back the deformation back to the fluid solver, resulting in increase in the lift and therefore increase in the displacement.

Compared to the undamaged case; the maximum deformation of the fin is increased by 20% at the end of two way analysis. It is because the delaminated part of the upper ply separates under the effect of the suction pressure. In addition, as in the case of one-way analysis further separation in the cohesive zone is not observed.

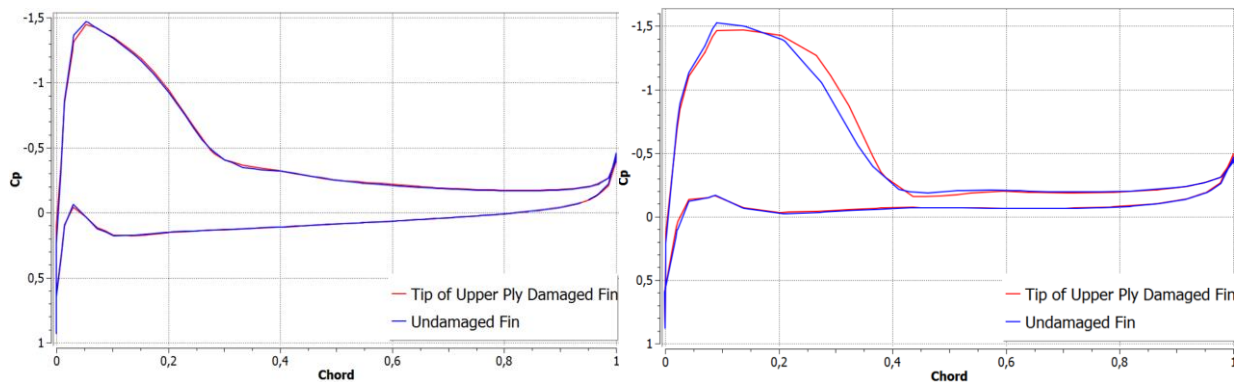


Figure 18: C_p distribution the Fin with Delamination in the Upper Ply Interface of the Fin Tip vs Undamaged Fin at the 50% (left) and 96% (right) span locations

Figure 18 shows that, C_p distributions for undamaged and damaged composite fin are nearly the same with each other at the half span location. However, at the span location that is close to the tip, the increase in the suction pressure for the damaged fin becomes more explicit due to the separation at the tip.

Delamination in Upper Ply Interface of the Trailing Edge of the Fin:

In this case, delamination is modeled by leaving a width of 20 mm from the trailing edge of the upper ply open while the remaining portion is bonded with cohesive elements and cohesive material properties given in Table 4 are used for the cohesive elements. Cohesive zone is placed between the upper ply and the second ply as shown in Figure 19.

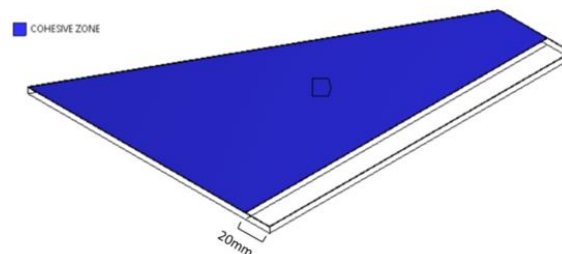


Figure 19: Trailing Edge Delamination Model

Convergence history of the lift coefficient of the rigid and composite fin with trailing edge delamination is shown in Figure 20.

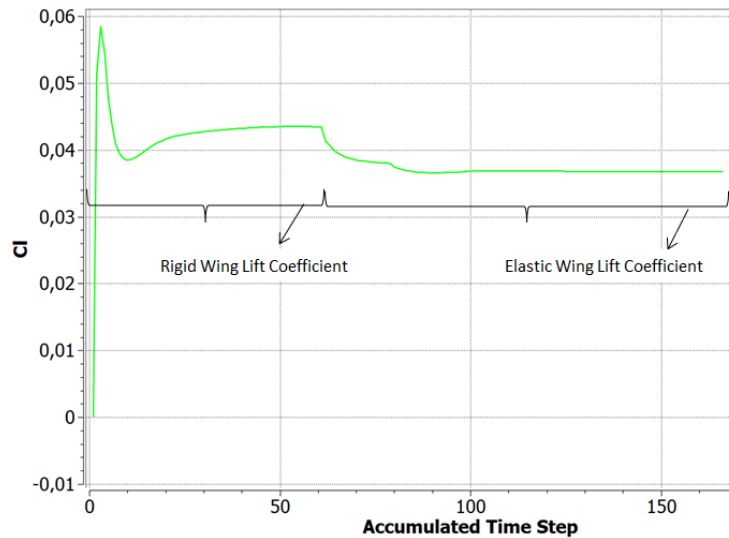


Figure 20: Convergence History of the Lift Coefficient of the Rigid and the Elastic Fin with Trailing Edge Delamination

It can be seen in Figure 20 that for the trailing edge delamination case there is a considerable decrease in the lift coefficient compared to the rigid one. The lift coefficient of the rigid fin is obtained as 0.0434 while the composite fin with trailing edge delamination is obtained as 0.0367. There is 15.44% decrease in the lift coefficient.

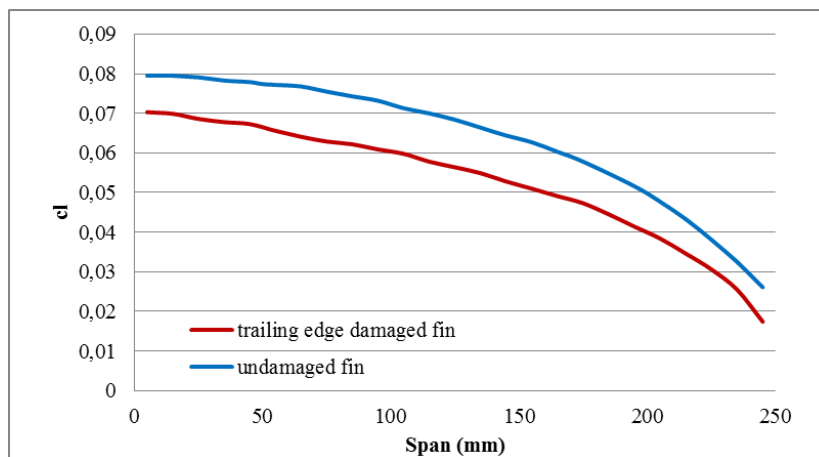


Figure 21: Spanwise Lift Coefficient of the Undamaged Fin vs. the Fin with Trailing Edge Delamination

The spanwise lift coefficients of the undamaged fin and the damaged composite fin with trailing edge delamination are shown in Figure 21. It is seen that, trailing edge delamination leads to a decrease in the overall lift distribution.

The converged maximum deformation of the damaged fin is 8.3 mm which is shown in Figure 22. It is to be noted that for the fin with trailing edge delamination, trailing edge of the fin deflects more compared to the leading edge resulting in decrease in the effective angle of attack. Reduction of the angle of attack causes the reduction in the lift distribution for the fin with trailing edge delamination.

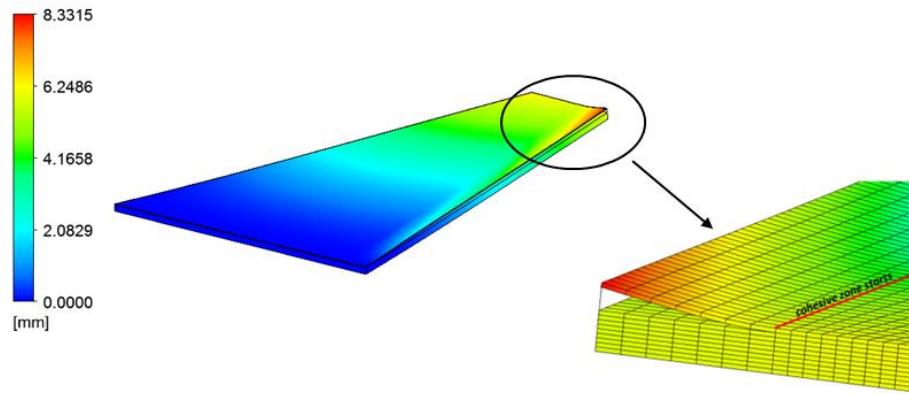


Figure 22: Aeroelastic Deformation of the Fin with Trailing Edge Delamination

In one way analysis, the maximum deformation of the fin with delamination along the trailing edge of the upper ply was found as 10.2 mm. As a result of the two way analysis, decrease in lift leads to decrease in the maximum deformation by 18.4 %. It is noted that, maximum deformation of the fin with trailing edge delamination is closer to the deformation of undamaged fin. The maximum displacement is due to the separation of the delaminated part on the upper ply. However, at the end of two-way analysis, further separation in the cohesive zone is not observed.

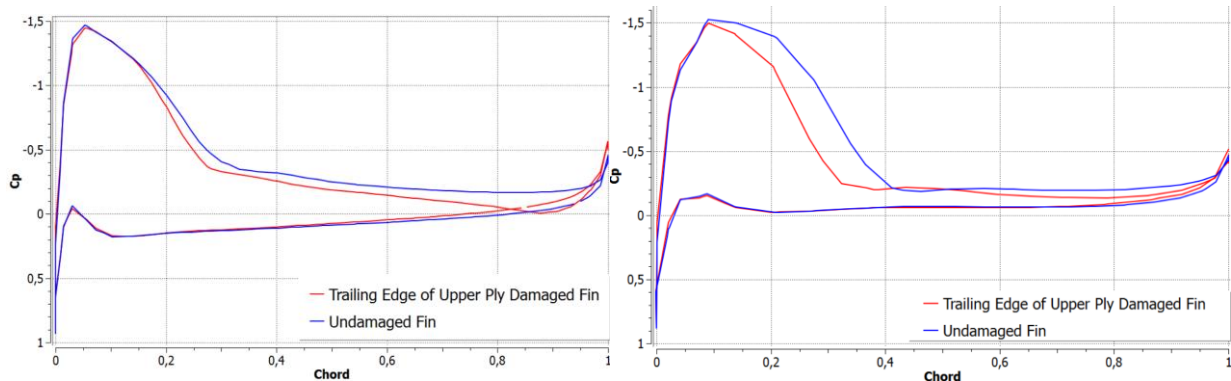


Figure 23: C_p distribution the Fin with Delamination in the Upper Ply Interface along the Trailing Edge of the Fin vs Undamaged Fin at the 50% (left) and 96% (right) span locations

Figure 23 shows that, suction pressure on the upper surface of damaged fin is lower than the undamaged one. Reduction of the suction pressure leads to a decrease in lift. In addition, in Figure 23, the irregular C_p distribution in the damaged location is noticeable at 50% span location.

Delamination in Upper Ply Interface of the Leading Edge of the Fin:

In this case, delamination is modeled by leaving a width of 20 mm from the leading edge of the upper ply open while the remaining portion is bonded with cohesive elements and cohesive material properties given in Table 4 are used for the cohesive elements. Cohesive zone is placed between the upper ply and the second ply as shown in Figure 24.

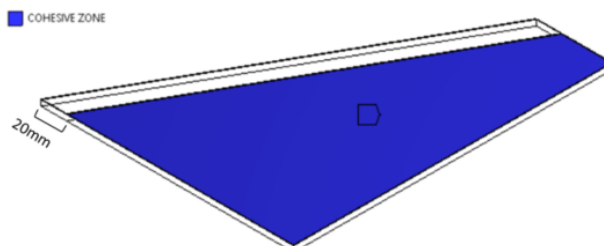


Figure 24: Leading Edge Delamination Model

Convergence history of the lift coefficient of the rigid and the composite fin with leading edge delamination is shown in Figure 25.

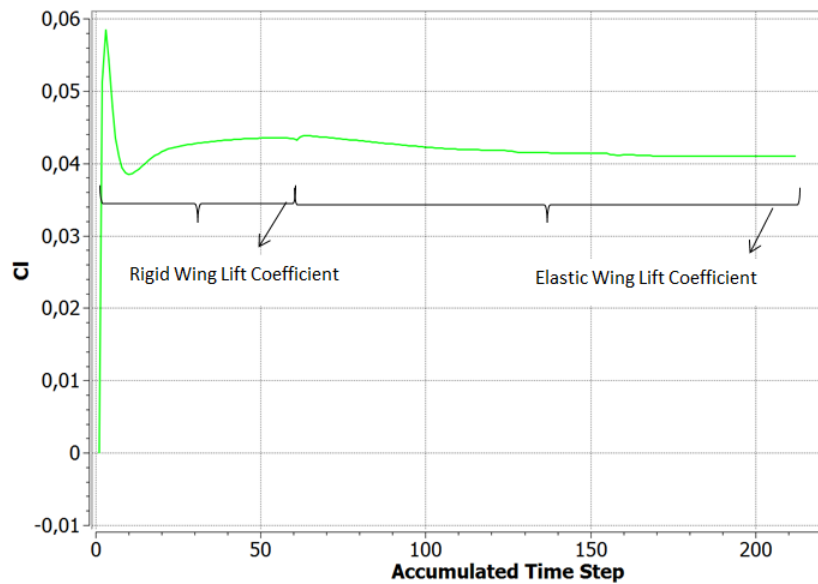


Figure 25: Convergence History of the Lift Coefficient of the Rigid and the Elastic Fin with Trailing Edge Delamination

For the leading edge delamination case, there is a decrease in the lift coefficient compared to the rigid one. The lift coefficient of the rigid fin is obtained as 0.0434 while the lift coefficient of the damaged elastic fin is obtained as 0.0410. In this case, there is 5.5% decrease in the lift coefficient.

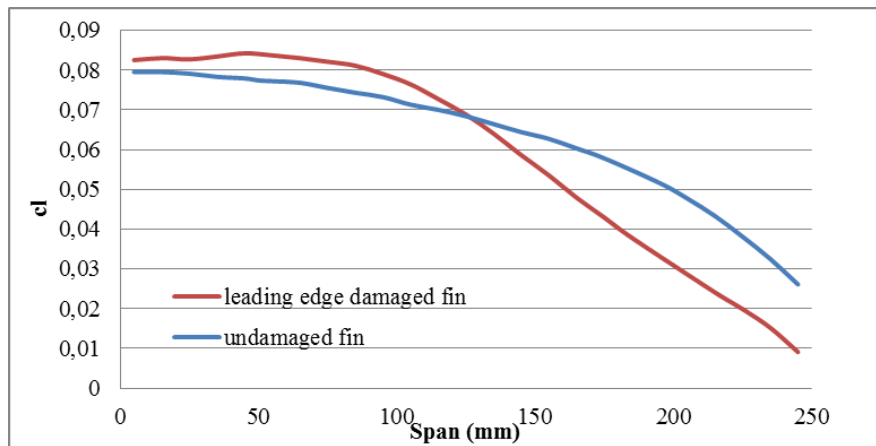


Figure 26: Spanwise Lift Coefficient of the Undamaged Fin vs. the Fin with Leading Edge Delamination

The spanwise lift coefficient of the undamaged fin and the fin with delamination in the leading edge of the fin is shown in Figure 26. Figure 26 shows that the lift coefficient is higher from root to half of the span but it starts to decrease beyond approximately the half span location. However, the resultant lift coefficient is less than the rigid one as seen in Figure 25. The converged maximum deformation of the fin is 7.7 mm which is shown in Figure 27.

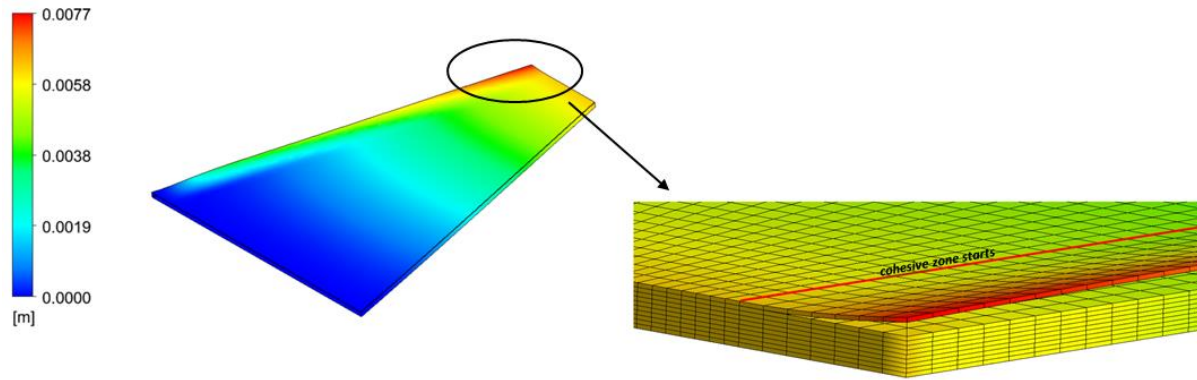


Figure 27: Aeroelastic Deformation of the Fin with Leading Edge Delamination

In one way analysis, the maximum deformation of the fin that has delamination in the leading edge was found as 10.9 mm. The decrease in lift at the end of two way analysis results in a decrease in the maximum deformation. It is to be noted that the resulting deformation of the fin is lower than the undamaged fin. The maximum displacement is due to the separation of the delaminated part on the upper ply. However, at the end of two-way analysis, further separation in the cohesive zone is not observed, as in the other cases. Figure 28 compares the C_p distribution of the fin with delamination in the upper ply interface of the leading edge of the fin with the undamaged fin at three locations along the span of the fin.

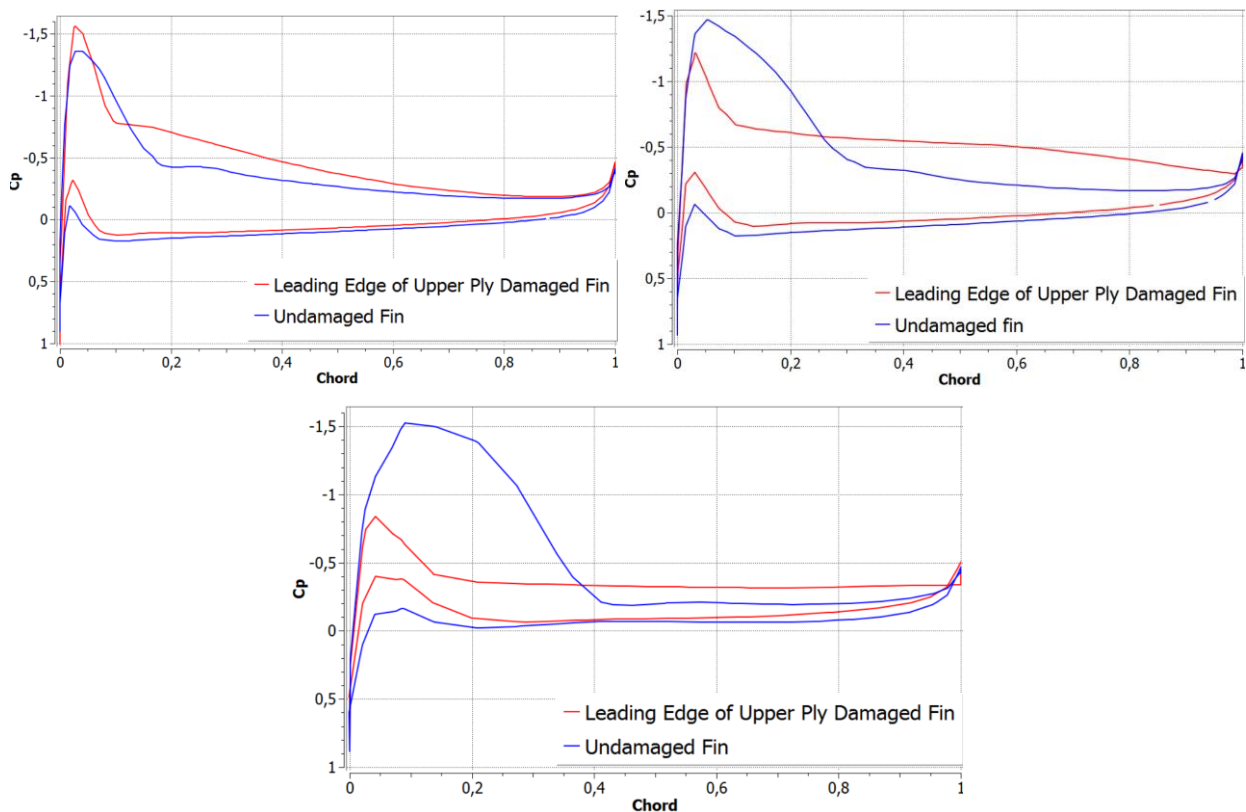


Figure 28: C_p distribution of the Fin with Delamination in the Upper Ply Interface of the Leading Edge of the Fin vs Undamaged Fin at the 22% (left), 50% (right) and 96% (bottom) span locations

Figure 28 shows that at the 22% span location from the root, suction pressure is higher for the damaged fin than the undamaged fin. However at the 50% and 94% of the span locations, there is a significant decrease in the suction pressure at the leading edge side of the fin.

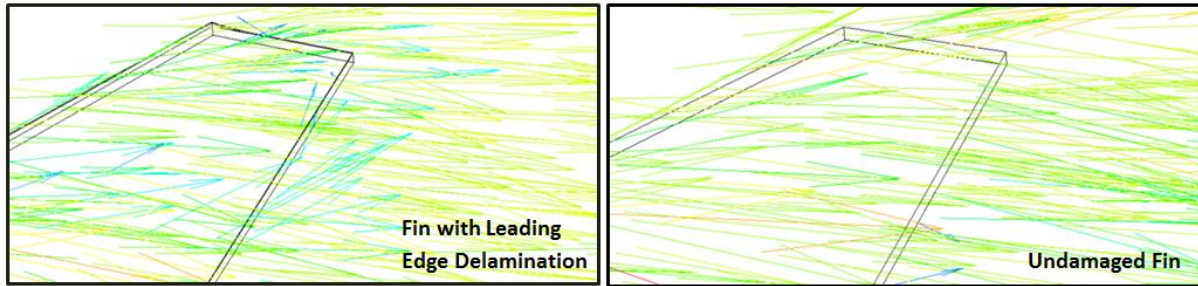


Figure 29: Velocity Vectors of the Flow around the Fin

The overall decrease of the lift coefficient given in Figure 25 is attributed to the following reasons. Towards the trailing edge of the fin with leading edge delamination, suction pressure increases, compared to the undamaged fin. The increase in the suction pressure is considered to be due to the increase of the effective angle of attack of the fin due to the higher deflection of the leading edge of the fin compared to the trailing edge of the fin, as seen in Figure 27. However, under the aerodynamic loading, separation of the upper ply from the rest of the laminate apparently distorts the aerodynamic flow near the leading edge. Figure 29 shows the distortion in the flow for the fin with delamination along the leading edge of the upper ply interface. Higher deflection of the upper ply from the rest of the laminate along the outboard leading edge of the fin distorts the aerodynamic flow more compared to the inboard leading edge resulting in the decrease in the spanwise lift distribution, as shown in Figure 26. In the end, combined effect of the increase in the effective angle of attack of the fin sections due to the deflection of the fin and distortion of the aerodynamic flow near the leading edge of the fin due to the delamination causes reduction in the total lift coefficient, as shown in Figure 25.

CONCLUSION

Nonlinear static aeroelastic analysis of a composite fin with interlaminar damage is performed using two way coupled approach. The aim of this research was to investigate the effects of damages in composites with coupled effects of flowing fluid and a simplified composite fin by using a two-way fluid-structure interaction. The capability of two-way fluid-structure interaction modeling available in the commercial software ANSYS was used in this study. The method is verified by two way FSI analysis of the generic AGARD 445.6 wing. The mesh size study is performed and the results show a good agreement with the results available in literature.

The FSI method verified in AGARD 445.6 wing case is then applied to simplified composite fin geometry with the same flow condition. Interlaminar failure is created in the composite fin by placing delamination and cohesive interface between the plies in the upper face of the fin which is under compression as a result of the aerodynamic loading. Different regions such as the tip, leading edge and trailing edge of the missile fin are left open to simulate the delamination while the rest of the laminate is kept bonded with cohesive elements. The properties of the cohesive elements are taken from the study of Travesa [Travesa, 2006] and the bilinear cohesive zone material model that is used for the analysis is validated by comparing the results with Travesa [Travesa, 2006].

At the end of two way analysis, it is seen that there is no significant difference between the lift and pressure distribution of undamaged fin compared to rigid one. In addition, the results of one way and two solutions give almost the same results. It is because the missile fin studied is relatively rigid. It can be said that for an undamaged composite fin, the effect of deformation of the fin on the flow can be ignored.

As the first delamination case, cohesive interface is placed in the upper ply interface by leaving 10% of the ply open from the tip. At the end of two way analysis, it is seen that there is a little increase in the lift compared to the undamaged case. The delamination of the tip results in an increase in effective angle of attack this location resulting in the increase of the lift. At the end of two way analysis, no separation is observed in the cohesive zone and the increase in stress and deformation is not so different than the one way solution. Therefore,

same with undamaged fin case, it can be said that, for a fin with delamination in the upper ply interface of the tip, the effect of deformation of the fin on the flow can be ignored.

In the case of fin with delamination in the upper ply interface of the trailing edge, delamination is modeled by leaving a width of 20 mm from the trailing edge of the upper ply open while the remaining portion is bonded with cohesive elements. At the end of two way analysis, it is seen that there is a considerable decrease in the lift of the fin. The separation of the upper ply along the trailing edge makes the trailing edge deflection more than the leading edge. Therefore, the reduction of the effective angle of attack causes the reduction in the lift distribution. Consequently, the reduction in lift distribution results in a decrease in the maximum deformation of the fin compared to the one way analysis.

The third interlaminar failure case studied is the delamination along the leading edge of the fin. In this case, delamination in the upper ply interface of the leading edge is modeled by leaving a width of 20 mm from the leading edge of the upper ply open while the remaining portion is bonded with cohesive elements. The results show that while at the inboard sections lift distribution is higher than the undamaged fin, at the outboard sections lift decreases drastically. This behavior is attributed to the distortion of the flow due to the separation of the delaminated ply from the rest of the laminate. However, at the inboard sections increase in lift results from an increase in effective angle of attack due to the higher deflection of the leading edge of the fin than the trailing edge of the fin. However, for the leading edge delamination case, overall lift is reduced as well as the maximum deformation compared to the undamaged fin.

From the three delamination cases investigated, it is seen that delamination in the upper ply interface of the tip is not an important issue as the trailing edge and the leading edge delamination. From aeroelastic effect point of view, leading edge and trailing edge delamination, which are very probable due to manufacturing of the composite fin or during the operation of the missile, are considered to be more critical. Moreover, delaminations in the interfaces of the composite laminate which are under compression are determined to be more critical in terms of the effect of the delamination on the aeroelastic response of the missile fin. It should be noted that especially leading edge delamination is very probable due to the flow impinging on the leading edge during flight of the missile. Metal or ceramic shielding on the leading edges and trailing edges may be required make sure that there is no delamination in these regions.

References

Ansys Inc. (2013) *Ansys Mechanical APDL Theory Reference Guide*.

Ansys Inc. (2013) *Ansys CFX Solver Reference Guide*.

Bauchau O.A., Loewy R. G. (1997) *Nonlinear Aeroelastic Effects in Damaged Composite Aerospace Structures*, Defense Technical Information Center, Oct 1997.

Cai J., Liu F., Tsai H.M., Wong A.S.F. (2001) *Static Aero-elastic Computation with a Coupled CFD and CSD Method*, AIAA 2001-0717, Aerospace Sciences Meeting and Exhibit, 39th, Reno, NV, Jan 2001.

Eastep, F.E. Venkayya, V.B. and Tishler V. A. (1984) *Divergence Speed Degradation of Forward-Swept Wings with Damaged Composite Skin*, Journal of Aircraft, Vol. 21, No. 11, pp. 921–923, November 1984.

Kim T., Atluri S.N. and Loewy R.G. (1998) *Modeling of Microcrack Damaged Composite Plates Undergoing Nonlinear Bimodular Flutter Oscillations*, AIAA Journal, 36(4), 598–606.

Strganac T.W., and Kim Y.I. (1996) *Aeroelastic Behavior of Composite Plates Subject to Damage Growth*, Journal of Aircraft, Vol. 33, No. 1, pp. 68–73, January-February 1996.

Travesa A. T. (2006) *Simulation of Delamination in Composites Under Quasi-Static and Fatigue Loading Using Cohesive Zone Models*, Dr. Thesis, p. 218.

Wang K., Inman D. J., Farrar C. R. (2005) *Crack-induced Changes in Divergence and Flutter of Cantilevered Composite Panels*, Structural Health Monitoring, December 2005.

Wang K. and Inman D.J. (2007) *Crack-Induced Effects on Aeroelasticity of an Unswept Composite Wing* Publisher, AIAA JOURNAL Vol. 45, No. 3, March 2007.

Yates E.C. (1995) *AGARD Standard Aeroelastic Configurations for Dynamic Response*, AGARD Report No .765, Meeting of the Structures and Materials Panel at Oberammergau, Germany, September 1995.